

Predictive Gold Nanocluster Formation Controlled by Metal-Ligand Complexes

John M. Pettibone* and Jeffrey W. Hudgens*

*The formation of ligand-protected gold nanoclusters during size-selective syntheses is seemingly driven by the inherent properties of the protecting ligands, but a general description of the product formation has not been presented. This study uses diphosphine-protected Au clusters as a model system to examine i) control of metal-ligand complex distributions in methanol–chloroform solutions, ii) role of solution perturbations, e.g., oxidation, and iii) nanocluster formation through reduction of characterized complex distributions. By selectively reducing complexes and monitoring cluster formation with electrospray ionization mass spectrometry and UV–vis, data show the distribution of complexes can be controlled through ligand exchange, and the reduction of specific complexes produce characteristic ligated gold clusters based on ligand class. Specifically, 1,*n*-bis(diphenylphosphino)*n*-alkane ligands, L^n , where $n = 1$ through 6, are classified into two distinct sets. The classes represent ligands that either form mainly $[AuL^n_2]^+$ (Class I, $n = 1–3$) or bridged $[Au_2L^n_2]^{2+}$ (Class II, $n = 4–6$) complexes after complete ligand exchange with $AuClPPh_3$. Selectively reducing gold-phosphine ligand complexes allows mapping of product formation, resulting collectively in a predictive tool for ligated gold cluster production by simply monitoring the initial complex distribution prior to reduction.*

1. Introduction

Extensive resources are devoted to parameterizing and optimizing monolayer-protected cluster (MPC) syntheses with the objective of developing generalized methods that produce predictable, monodisperse products. The development of synthetic methods that result in monodisperse nanocluster formation is of fundamental importance for the characterization of size–property relationships, and nearly pure MPCs can be used as molecular building blocks for new materials. Kinetic models have been developed to identify nucleation, growth and formation of clusters and nanoparticles,

but these models contain little chemical information, likely limiting their predictive capability. Experiments are needed that follow single-product formation of different species, promoting the development of models for aimed syntheses.

The reduction of Au^I :phosphine complexes can produce narrow distributions of ligated-gold clusters.^[1–3] The production of monodisperse nanocluster distributions has been reported through two different methods that include controlled reduction and nucleation^[2,4] and postreduction solution-phase processing.^[1,5–7] The formation of monodisperse nascent products controlled by initial conditions can also facilitate more facile routes to desired products by implementing additional solution-phase processing methods. Two methodologies of postreduction solution-phase processing, “size-selective processing”^[3] and “size-focusing”,^[7] are known to facilitate the production of monodisperse cluster distributions. “Size-selective” defines the cyclic processing around stable nuclearities while “size-focusing” is defined as resistance by the most stable species to degradation. Both methodologies act to produce monodisperse product

Dr. J. M. Pettibone, Dr. J. W. Hudgens
Material Measurement Laboratory
National Institute of Standards and Technology
Gaithersburg, MD, 20899, USA
E-mail: john.pettibone@nist.gov; jeffrey.hudgens@nist.gov



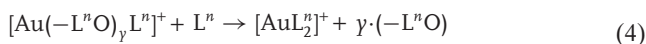
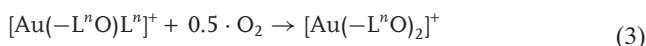
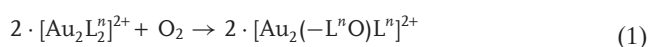
DOI: 10.1002/sml.201101777

distributions in aerated Au:diphosphine synthesis solutions.^[1,2,5,8] Furthermore, postreduction, solution-phase processing can promote geometric core rearrangement not easily accessible through initial synthetic methods,^[6] but application requires some knowledge of the reaction system. Protecting ligands such as thiols, polymers, amines, and phosphines have shown efficacy for producing monodisperse products and metal cluster etching,^[3,9–12] therefore, these ligands are candidates for facilitating size-selective syntheses of transition metal clusters.

Specifically for diphosphine ligands, Bertino et al.,^[1] reported some propensity for monodisperse, gold MPC formation with the incorporation of different L^n , $L^n = 1, n$ -bis(diphenylphosphino) n -alkane. A follow up computational study by Hong et al.,^[13] examined overall nanocluster stability and selectivity with diphosphines containing spacers of different lengths. This work found that that diphosphines, such as L^3 , can selectively stabilize clusters of specific gold nuclearity. However, they conclude that the conditions that make selectivity possible are more complex than stabilization alone. Their work encourages further experimental investigation into a chemical understanding of the reactions leading to monodisperse products.

To address the lack of chemical understanding, we have identified a significant portion of the active reaction networks in the size-selective processing for the Au: L^3 and Au: L^5 systems that show a propensity to form size-selected products.^[1,4,14] The final products are built from distinct nascent reduction-nucleation products, aka cluster platforms. The initial distributions of the complexes are observed to affect product formation. More recently, we have presented further work that supports a relationship between the initial (prior to reduction) metal-ligand complex distribution and diphosphine-protected Au_x cluster formation.^[2] By manipulating the initial distribution of Au^I: L^6 complexes, we demonstrated size-selective syntheses for L^6 -protected Au₈, Au₉, and Au₁₀ clusters. Bergeron et al.,^[8] reported that diphosphine ligand exchange reactions with AuClPPh₃, containing increasing equivalents with L^n , affect the distribution of complexes, but additional experiments were necessary to understand how to develop control. To date, a general relationship describing the inherent ligand properties controlling the initial distribution of complexes and subsequent nanocluster formation has not been developed and is the scope of the current study.

To examine the relationship between initial gold complexes and products, it is necessary to understand how to control the distribution of complexes being reduced. We have recently provided evidence that the relative abundances of each complex can be significantly affected by the presence of oxidative environments (ambient conditions).^[4] For example, experiments with equimolar solutions of L^5 and AuClPPh₃ were interpreted as evidence that oxidation changes the relative concentration of $[Au_2L_5]^{2+}$ and result in quantifiable changes in product formation.^[4]



where $-L^nO$ represents a L^n that has a single oxidized phosphine terminus. Reversible reactions were not readily observed after the formation of $[AuL_2^n]^+$ in the current reaction conditions. Examination of the formation and fate of other $[Au_2L_2^n]^{2+}$ complexes through the isolation of specific formation channels with different ligands is needed to more fully understand the relationship between complex distribution and product formation.

The current study examines the general relationship between the initial metal-ligand complex distribution and the cluster products observed after selective reduction of Au: L^n complexes. Diphosphine ligands are divided in two specific classes based the principal complex forming through ligand exchange, $[AuL_2^n]^+$ (Class I) and $[Au_2L_2^n]^{2+}$ (Class II), where complex formation is partially controlled by the steric constraints of each of ligand. The principal clusters observed in this study are illustrated in **Figure 1**. Reduction of Class I and Class II complexes yields distinct nuclearity nanoclusters that are similarly classified. We can qualitatively distinguish structural differences between complexes with the same stoichiometry. Therefore, this study examines how the inherent properties of the ligands control the structural properties of complexes and, in turn, cluster formation. The selective reduction is initiated by NaBH₄ addition, a relative fast reducing agent, which allows separate examination of both nascent

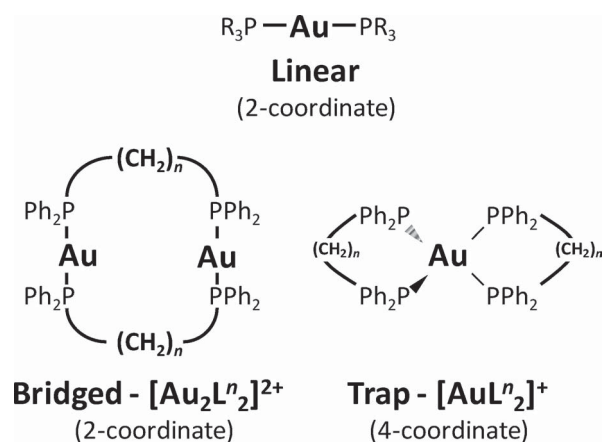


Figure 1. General structure of the principal complexes that form through ligand exchange with AuClPPh₃ and L^n . The linear complex can be $[AuL_2^n]^+$, $[AuL^n PPh_3]^+$ or $[Au(PPh_3)_2]^+$. The distribution and structure of the complexes are driven by the inherent properties and molar excess of each L^n that can be classified by the predominant complex forming at increasing diphosphine ligand concentrations, where Class I and Class II ligands form predominantly monogold or bridged complexes, respectively. The coordination number controls the relative rate of reduction of each complex.

product distributions and product distributions that evolve after subsequent solution phase processing.

By mapping the initial complex distribution to nanocluster products, we can develop *predictable syntheses* that simply rely on controlling the distribution of complexes existent prior to reduction. Further control of the ligated nanocluster distribution can be achieved via solution-phase processing. We believe that the approach presented here that classifies the metal-ligand precursors and final products can be extended to classifications for other metal-ligand systems initiated by reduction.

2. Results and Discussion

The following sections describe the experiments we use to outline the general relationship between the Au:Lⁿ complexes and the production and dispersity of ligated gold clusters. We provide the full complex distributions that form through increasing addition of Lⁿ, *n* = 1–6, to methanol–chloroform solutions containing AuClPPh₃ (10.0 ± 0.1 mg), which will be notated as [Lⁿ]/[PPh₃] from herein. Previous studies have reported the distributions of complexes for a limited range of [Lⁿ]/[PPh₃], Lⁿ, *n* = 1–3, 5 and 6, in the presence of O₂.^[1,2,15] We provide a complete experimental data set necessary for the development of a general classification of the complexes. The steric properties of the phosphine ligands in metal-ligand complexes have been extensively studied Lⁿ, *n* = 1–4, because they strongly contribute to their catalytic rate and selectivity.^[16–18] The inherent steric properties and the concentration of the ligands in solution control the distribution of Au:phosphine complexes. Specific complexes are susceptible to oxidation, altering the distribution of complexes and affecting product formation. Measurements of distributions of complexes are not remarkable as standalone data, but these data allow the development of relationships among the initial complexes and reduction products. By selectively reducing complexes we develop a tool that can be used to predict the product formation from all known distributions of gold-Lⁿ complexes.

2.1. Distributions of Gold-Diphosphine Ligand Complexes in Methanol–Chloroform

Prior to reduction, ligand exchange processes involving the AuClPPh₃ precursor and Lⁿ control the complex distribution in solution. A trend in the amount of the Lⁿ equivalents needed to replace PPh₃ from the AuClPPh₃ precursor is controlled by the carbon backbone chain length, with the longer chain ligands requiring more equivalents of Lⁿ to completely displace PPh₃. This distribution subsequently affects product formation; therefore, examination of the initial processing of the precursor in solution is necessary.

Electrospray ionization mass spectrometry (ESI-MS) data for AuClPPh₃ in solution display a weak peak representative of [Au(PPh₃)₂]⁺. Additional PPh₃ significantly increases the total ion current (TIC) dominated by [Au(PPh₃)₂]⁺, because phosphine ligands promote the dissociation of the AuClPPh₃

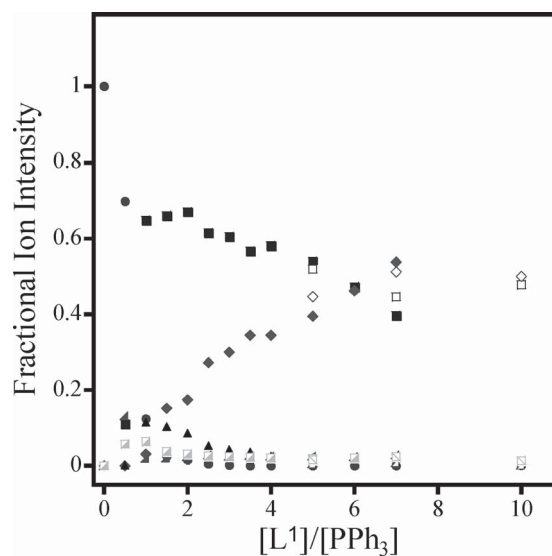


Figure 2. Fractional ion intensity of complexes in solution with increasing [L¹]/[PPh₃] represented by: circle [Au(PPh₃)₂]⁺, triangle [AuL¹(PPh₃)₂]⁺, diamond [AuL¹]⁺, solid square [Au₂L¹]₂²⁺, split square [Au₂L¹Cl]⁺, wedge [Au₃L¹Cl₂]⁺. Deaerated solutions for the same Au:L¹ complex are hollow points (e.g., [AuL¹]⁺ is represented by solid diamond (◆) and hollow diamond (◇) for aerated and deaerated solutions, respectively).

precursor through ligand exchange. The TIC reaches its maximum intensity after ~3 molar excess of PPh₃ (i.e., 2 molar equivalents of PPh₃ and 1 equivalent from AuClPPh₃), and the TIC remains constant for [PPh₃]/[Au¹] > 3. Therefore, excess phosphine ligands in solution will affect both the amount of cationic species in solution (ionic strength) and the distribution of complexes. Addition of two molar equivalents of diphosphine ligands also results in the maximum TIC observed. The extent of ligand exchange on AuClPPh₃ with excess phosphine ligands is reported to affect MPC formation,^[2] indicating that understanding (or at least monitoring) the ligand exchange reactions is necessary for predicting product formation.

Guided by these findings given above, we investigate the complete ligand exchange and dissolution of the AuClPPh₃ precursor with multiple diphosphine ligands, Lⁿ, where *n* = 1 to 6. **Figure 2** shows the relative abundance of complexes as a function of [L¹]/[PPh₃]. At the lowest relative ratio of L¹, the [Au(PPh₃)₂]⁺ complex dominates the TIC in the ESI-MS spectrum. Smaller amounts of [Au₂L¹]₂²⁺, [Au₂L¹Cl]⁺ and [Au₃L¹Cl₂]⁺ are also observed. Based on the phosphorous equivalents, we expect that undissociated AuClPPh₃ remains in solution (vide supra). With increasing [L¹], [Au₂L¹]₂²⁺ species dominate the spectra and constitute greater than half of TIC at [L¹]/[PPh₃] < 5, consistent with previous results.^[15] [Au(PPh₃)L¹]⁺ is present in the highest fractional ion intensity at [L¹]/[PPh₃] ≈ 1 and decreases with increasing [L¹]. With increasing ratios above [L¹]/[PPh₃] ≈ 1, [AuL¹]⁺ increases with a fractional ion intensity similar to the ion intensity for [Au₂L¹]₂²⁺ at [L¹]/[PPh₃] ≥ 6. A concurrent decrease of the PPh₃ and Cl⁻ containing complexes occurs with increasing concentrations of [AuL¹]⁺. At [L¹]/[PPh₃] ≥ 6, the solution is dominated by the [AuL¹]⁺ and [Au₂L¹]₂²⁺ complexes with

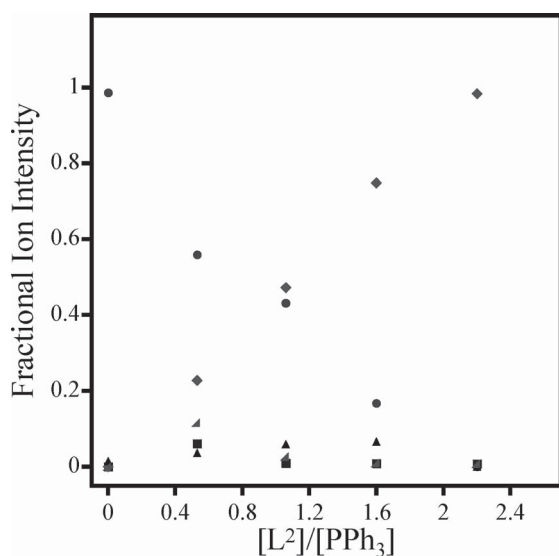


Figure 3. Fractional ion intensity of complexes in solution with increasing $[L^2]/[PPh_3]$ represented by: circle $[Au(PPh_3)_2]^+$, triangle $[AuL^2(PPh_3)]^+$, diamond $[AuL^2]^+$, square $[Au_2L^2]^{2+}$, wedge $[Au_3L^2Cl_2]^+$.

only small signal intensities of the chlorinated $[Au_2L^2Cl]^+$ and $[Au_3L^2Cl_2]^+$ present. In general, the L^1 ligand does not chelate to the metal center, as this structure forms a thermodynamically unfavorable four-membered ring. Instead, the digold L^1 complexes are almost always a bridged species.^[19] Below we present data supporting a linear structure for $[AuL^1]^+$.

For L^2 complexes, complete ligand exchange of PPh_3 on $AuClPPh_3$ occurs at much lower molar equivalents of the L^2 , as compared to L^1 (Figure 3). At low relative molar ratios of L^2 , $[L^n]/[PPh_3] \leq 0.5$, $[Au(PPh_3)_2]^+$ is the salient feature in the ESI-MS spectra with smaller signal intensities from $[AuL^2]^+$, $[Au_2L^2]^{2+}$, $[Au_2L^2Cl]^+$, and $[AuL^2(PPh_3)]^+$. In contrast to L^1 , the $[Au_2L^2]^{2+}$ complex is never the dominant species; instead, the $[AuL^2]^+$ always exhibits the highest fractional ion intensity of L^2 containing complexes, and it is the only measured signal at $[L^2]/[PPh_3] \geq 2.5$.

The evolution of the $Au:L^3$ complex distribution is similar to L^2 , but it has distinct differences in the distribution of complexes that form (Figure S1, Supporting Information (SI)). With increasing $[L^3]/[PPh_3]$ we observe an increase of $[AuL^3]^+$, which has a reported crystal structure of a four-coordinate Au^I species.^[20] Chlorinated and heteroleptic complexes are also present. The amount of L^3 added to drive complete ligand exchange is $[L^3]/[PPh_3] \approx 2$, consistent with previous studies,^[8,15] but both $[AuL^3]^+$ and $[Au_xL^3_x]^{x+}$ complexes are present in deaerated systems. Also, the relative intensity of the $[Au(PPh_3)L^3]^+$ is greater for L^3 than L^1 and L^2 , which affects cluster formation (vide infra).

With differences present for the aerated and deaerated systems, the role of ambient conditions is examined and compared to the predicted degradation pathways in reactions 1–4. When comparing fractional ion intensities in the L^1 system, little change in the ESI-MS signal intensity is observed between aerated and deaerated systems (Figure 2). The structure of $[Au_2L^1]^{2+}$ could be an oligomeric chain of

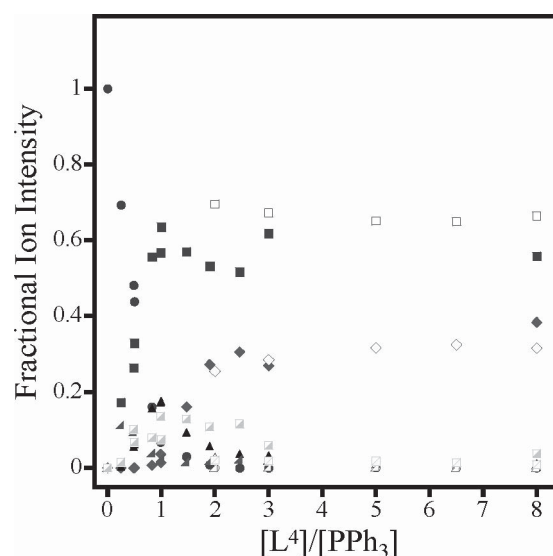


Figure 4. Fractional ion intensity of complexes in solution with increasing $[L^4]/[PPh_3]$, where complexes are represented by: circle $[Au(PPh_3)_2]^+$, triangle $[AuL^4(PPh_3)]^+$, diamond $[AuL^4]^+$, solid square $[Au_2L^4]^{2+}$, split square $[Au_2L^4Cl]^+$, wedge $[Au_3L^4Cl_2]^+$. The unfilled shapes represent data for deaerated solutions (e.g., fractional ion intensity of $[AuL^4]^+$ is represented by solid diamond (\blacklozenge) and hollow diamond (\diamond) for aerated and deaerated solutions, respectively).

two coordinate Au atoms bridged by L^1 .^[21] For L^2 , $[Au_2L^2]^{2+}$ is only a minor component of the distribution with the maximum fractional ion intensity at $[L^2]/[PPh_3] \sim 0.5$. The growth in the fractional ion intensity of the $[AuL^2]^+$ complex is almost linear with increasing $[L^2]/[PPh_3]$ and almost no change is observed in aerated systems. In brief, the distributions of $Au:L^1$ and $Au:L^2$ complexes are not strongly affected by ambient conditions.

The distribution of complexes in the deaerated $Au:L^3$ systems (Figure S1, SI) shows an increase in the fractional ion intensity of the $[Au_2L^3]^{2+}$ compared to $Au:L^2$ systems. This observation differs from previously reported distributions in aerated systems,^[8] indicating that oxidation affects the complex distribution. $[Au_2L^1]^{2+}$ and $[Au_2L^2]^{2+}$ are less susceptible to oxidation, as compared to $[Au_2L^3]^{2+}$, providing evidence for possible structural differences.

The distribution of complexes as a function of increasing $[L^4]/[PPh_3]$ (Figure 4) differs from the trends observed for L^n , when $n = 1, 2, 3$. Although $[Au(PPh_3)_2]^+$ dominates the TIC at $[L^4]/[PPh_3] \leq 0.5$, $[Au_2L^4]^{2+}$ signal increases with increasing $[L^4]/[PPh_3]$. At $[L^4]/[PPh_3] = 8$ the largest fraction of the TIC is $[Au_2L^4]^{2+}$, and a smaller fraction arises from $[AuL^4]^+$. As compared with aerated solutions, deaerated solutions exhibit an increased fractional ion intensity of $[Au_2L^4]^{2+}$, indicating that ambient conditions influence the complex distributions.

The evolution of $Au:L^5$ and $Au:L^6$ complex distributions exhibit trends similar to those observed for $Au:L^4$. As $[L^n]/[PPh_3]$ increases, the $[Au_2L^n]^{2+}$ ($n = 5, 6$) complex always accounts for the largest fraction of the TIC. Ambient environments promote the degradation of $[Au_2L^n]^{2+}$, resulting in increased concentrations of $[AuL^n]^+$ (not shown). Finally, compared to $Au:L^4$ and $Au:L^5$ systems, $Au:L^6$ solutions are

unique, as monogold complexes containing L^6 are absent from the ESI-MS. This observation is in accord with our previous results.^[2]

The ESI-MS data for L^4 complex distributions show the slow increase of the fractional ion intensity of $[AuL^4_2]^+$ with increasing exposure to ambient conditions. The continual addition of L^4 to stirring, capped solvent mixtures from $1 \leq [L^4]/[PPh_3] \leq 3$ results in diminishing fractional ion intensity of $[Au_2L^4_2]^{2+}$ and corresponding growth in $[AuL^4_2]^+$, indicating a degradation pathway for $[Au_2L^4_2]^{2+}$. The degradation of $[Au_2L^n_2]^{2+}$ outlined in reactions 1 through 4 describes the incorporation of O atoms into a diphosphine ligand (and not into the Au core), producing a phosphine oxide terminus. Comparison of the ambient exposed reaction vials with the deaerated system (open data points) in Figure 4 provides compelling evidence that oxidation affects the complex distribution in short time periods ($t < 10$ min). The deaerated solution displays a relatively unchanging complex distribution in the Au: L^4 system above $[L^4]/[PPh_3] \sim 2$.

Similar susceptibility of the complex distribution to aerated conditions is also apparent for Au: L^5 (not shown). Significant changes in Au: L^4 and Au: L^5 distributions indicate that these complexes are much more susceptible to oxidation than in the Au: L^1 , Au: L^2 , and Au: L^3 systems. These data indicate that reactions 1–4 are active for $[Au_2L^n_2]^{2+}$ complexes, where $n = 3$ to 6. Further discussion is found in the supporting information.

We examined the reversibility of the complex distribution in order to identify active reaction pathways that could be associated with perturbations from liberated ligands during reduction. For $[L^n]/[PPh_3]$ that form predominantly $[AuL^n_2]^+$, addition of PPh_3 did not significantly change the relative ion intensities observed in the ESI-MS spectra, indicating the system is not reversible

under current reaction conditions. Figure S2 (SI) shows the addition of PPh_3 ligands at similar $[L^2]/[PPh_3]$ after the complex distribution was driven to $[AuL^2_2]^+$, but no distinguishable change is observed in the ESI-MS spectra. Even after the addition of 50× molar excess (25 equivalents) of PPh_3 , only a small signal in the ESI-MS spectrum is observed for $[Au(PPh_3)L^2]^+$. Similarly, addition of excess PPh_3 to solutions containing $[AuL^3_2]^+$ does not result in the formation of large concentrations of PPh_3 -containing complexes (Figure S3A, SI). The data support the description of $[AuL^n_2]^+$ as a Au^I trap.^[8] Noteworthy, identification of all species is needed to accurately describe the system and determine equilibrium coefficients. These species will likely include neutral complexes that are not detected with conventional ESI-MS.

Schwerdtfeger et al.^[22] reported relativistic calculations for other possible stable neutral species involved in the solution equilibrium with $AuClPPh_3$. They predicted the formation of $AuClPPh_3$ dimers that are stabilized by strong dipole-dipole interactions between the H and Cl atoms; aurophilic interactions were reported negligible. Au: L^n (L^n , $n = 4$ to 6) solutions that form $[Au_2L^n_2]^{2+}$ complexes exhibit reversibility as PPh_3 is added, which is the behavior expected of a solution near equilibrium. For example, as a 50× molar excess of PPh_3 is added to a solution exhibiting predominately $[Au_2L^5_2]^{2+}$, $[Au(PPh_3)_2]^+$ and $[Au(PPh_3)L^5]^+$ complexes are observed to reform (Figure S3B).

With the collection of clear distinctions between the L^n ligands that form unique distributions of metal-ligand complexes based on the carbon backbone chain lengths, the ligands are assigned to distinct classes based on propensity to form either $[AuL^n_2]^+$ (Class I) or $[Au_2L^n_2]^{2+}$ (Class II) as described in **Table 1**. Class I includes L^n ($n = 1-3$) and Class II includes L^n ($n = 4-6$) with L^1 and L^6 having unique properties in their respective classes.

Table 1. Summarized parameters for bite angles of diphosphine ligands separated into classes.

	Ligand	Ring size	Solution complexes (FIC) ^{b)}	$[L^n]/[PPh_3]$ ^{c)}	Initial products	Bite angle [°] ^{d)}
Class I	$L^{1a)}$	4	~50% $[Au(L^1)_2]^+$ ~50% $[Au_2L^1_2]^{2+}$	N/A	Neutral clusters	72.59 (1.28) ^{e)} 71.71 (1.6) ^{f)}
	L^2	5	~100% $[AuL^2_2]^+$	2.2	Neutral clusters ^{g)}	85.46 (1.01) ^{e)} 85.03 (3.11) ^{f)}
	L^3	6	~70% $[AuL^3_2]^+$ ~27% $[Au_xL^3_x]^{x+}$	2.0	Neutral clusters ^{g)}	92.94 (1.95) ^{e)} 91.08 (4.00) ^{f)}
Class II	L^4	7	~35% $[AuL^4_2]^+$ ~65% $[Au_2L^4_2]^{2+}$	8.0	Cationic Au_8 and Au_{10}	96.81 (3.17) ^{e)} 97.70 (5.15) ^{f)}
	L^5	8	~15% $[AuL^5_2]^+$ ~85% $[Au_2L^5_2]^{2+}$	12.5	Cationic Au_8 and Au_{10}	92.44 ^{g),h)}
	L^6	9	~100% $[Au_2L^6_2]^{2+}$	—	Cationic Au_8 and Au_{10}	N/A ^{h)}

^{a)}The L^1 ligand is reported not to chelate because of the rigidity of the backbone forming unchelated $[Au(L^1)_2]^+$ species.^[19] ^{b)}Abundances are computed from the fraction of the TIC of each cation; standard deviations (2σ) do not exceed 10%; ^{c)}Upper limit at which reduction of complexes is inhibited in sealed ambient conditions; ^{d)}Values in parentheses represent reported standard deviation (1σ) from each reference; ^{e)}Reference [27]; ^{f)}Calculated values from reference [16]; ^{g)}Calculated ligand bite angles $P\bullet\bullet P$ from crystal data with bond distance of $Au\bullet\bullet P = 2.278$ from bite angle = $2\arcsin(0.5 [r_{P\bullet\bullet P}]/(Au\bullet\bullet P))$.^[27]; ^{h)}No value has been reported for a chelated ligand structure that is suitable for direct comparison with L^n , $n = 1$ to 4; ⁱ⁾Nascent neutral distribution is predominantly Au_8 and Au_9 clusters (see text).

2.2. Steric Contributions of Ligands Contributing to Formation of Complexes

The ability to clearly distinguish different classes of Au:diphosphine complexes is unexpected from an electronic perspective, but the split between classes is clearly observed for both the distribution of solution complexes and corresponding nascent reduction products (vide infra). The current study is designed to isolate structural (steric) contributions of ligands with similar electronic structure.^[23]

The bite angle is currently the most fully developed concept describing steric contributions of diphosphine ligands in metal-ligand complexes. It was first reported in the seminal work by Tolman^[24] on monophosphines and has been extended to incorporate diphosphines.^[25] The bite angle is defined as the angle between the bisecting vector of P–M–P chelating ligand and the M–P bond with additional contributions of the non-bridging substituent with dummy metal atoms for comparison.^[16,26] Further extensions of the bite angle concept have been presented to account for steric contributions that generalize the ligand contribution in different metal systems.^[26,27] A large amount of work has been conducted on diphosphine ligand-TM complexes with these measured steric contributions.^[16,17,26–29] In general, the change in the conformation of the complex structure from a square-planar or tetrahedral complex to an octahedral complex is observed when the bite angle of the phosphine changes from 90° to 120°, where ligand position is rearranged from equatorial to axial positions. Previous reported values of the bite angles for L¹ through L⁴ ligands (Table 1) give supporting evidence for the generalized trend of the coordination geometry. The classification of the ligands into Class I or Class II based on experimental observations of the predominant complex forming, [AuLⁿ₂]⁺ or [Au₂Lⁿ₂]²⁺, coincides with the change in the predicted stable structure of the complexes from tetrahedral/square-planar to octahedral geometries, based on ligand bite angle considerations. Therefore, the established bite angle concept provides a general descriptor for the steric contributions controlling the observed distribution of complexes.

A clear relationship is observed between increasing bite angle and forming complexes. However, steric properties of the ligands are not the only competing forces controlling structures of the complexes. The increasing length of the bridging carbon chain likely changes the contributions from competing forces, such as aurophilic interactions and entropic forces associated with increasing ligand flexibility (space filling). Aurophilic interactions may increase stabilization of metal-ligand complexes,^[30] which are attributed to correlation effects^[31,32] and are predicted to have similar energies to hydrogen bonding.^[33,34] Specifically, evidence for aurophilic interactions are reported in the bridged Au^I:L¹ systems, where the relative strength of the aurophilic interactions can be affected by solvent contributions and other complexing ligands.^[35,36] Schmidbaur and co-workers^[37] have also suggested that increased flexibility of phosphine ligands can promote aurophilic interactions, indicating that the relative contributions of aurophilic interactions in the Class I and Class II ligands are likely different. The observed difference in reduction efficiencies of the predominant complexes between

classes could also be affected by aurophilic contributions. Further computational and experimental studies examining the stability and structure of oxidized and reduced mono- and multi-gold complexes are needed to better understand how increasing bite angle (carbon chain length) changes the relative contributions from the competing forces that control structure.

Overall, the formation of complexes with Au^I and the diphosphines examined in the current study show a distinct shift in the complex distribution that corresponds to the predicted shift from tetrahedral or square-planar to octahedral geometry, as described by the bite angle of the ligands. Therefore, the classification of the complexes from Class I and Class II can be predicted by examining the steric contributions of the ligands,^[38] but further work is necessary to extend the bite angle concept or to support the development of a more appropriate measure of steric contributions for more flexible ligands, Lⁿ, n > 5.

2.3. Selective Reduction of Au:Lⁿ Complexes

The previous sections describe control over the initial complex distributions as a function of ligand concentration and environment. This section provides ESI-MS and UV-vis data that show a general relationship between the initial distribution of complexes and nascent product formation through selective reduction. Selective reduction can also provide information about structural differences between gold-ligand complexes with the same stoichiometry further distinguishing each class of Lⁿ. These relationships allow prediction of nascent product formation resulting from the reduction of specific distributions of complexes. Additional experimental evidence for controlled solution-phase processing on nascent cluster platforms is presented.

The amount of ligand exchange will strongly influence the reduction, nucleation and subsequent product formation of the ligated Au clusters. In general, the reduction reaction for monogold, Au^I-phosphine complexes is:



where [Au^ILL']⁺ is a ligated gold complex, *k*_{red} is the rate coefficient for reduction and [Au⁰LL'][•] is a free radical. Because the transition state for charge transfer comprises a borate species and [Au^ILL']⁺ engaged in complexation, the reduction rate of reaction 5 is partially dependent on the coordination number of the Au^I atom. Higher coordination putatively blocks available complexing sites for the reducing complex. Different reduction efficiencies (relative reaction rates) of the [AuLⁿ₂]⁺, [Au(PPh₃)₂]⁺, [Au(PPh₃)Lⁿ]⁺, and [Au₂Lⁿ₂]²⁺ were observed in our previous studies.^[4,14] Through selective reduction, we provide the first evidence that the rate for reaction 5 can be essentially lowered to zero by increasing the concentration of [AuLⁿ₂]⁺ for Lⁿ, n = 2 to n = 5. Note, reduction of the [AuL¹₂]⁺ is observed after NaBH₄ addition, resulting in a green solution that briefly persists prior to dark colloid formation. The Au:L⁶ systems do not produce

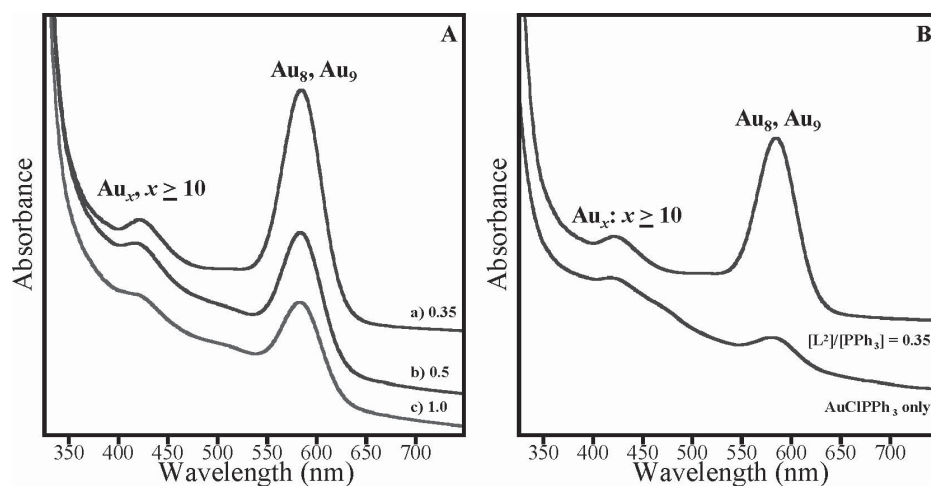
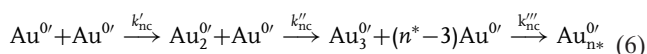


Figure 5. A) UV-vis spectra of the cluster distributions present at $[L^2]/[PPh_3] = 0.35, 0.5$ and 1.0 at $t \approx 15$ min after $NaBH_4$ reduction. The assayed solutions exhibit absorption bands at both 585 nm and 420 nm, indicating a distribution of PPh_3 -protected, neutral clusters are present. The 585 nm band results only from the presence of PPh_3 -protected Au_8 and Au_9 clusters, indicating that these are the predominant clusters present. With increasing L^2 equivalents, the overall peak intensity diminishes, consistent with increasing concentrations of the Au^I trap, $[AuL_2^2]^+$. B) The assayed solutions of Au^I reduction in the presence, $[L^2]/[PPh_3] = 0.35$, and absence of L^2 at $t \approx 15$ min. In the absence of L^2 , the relative intensity of 585 nm band is greatly diminished, indicating the majority of the distribution of neutral clusters is larger than Au_9 .

monogold complexes, and reduction is not completely inhibited at examined $[L^6]/[PPh_3]$ ratios ≤ 18 . These results indicate structural differences of the complexes that form in the $Au:L^1$ and $Au:L^6$ systems as compared to $Au:L^n$, $n = 2$ to 5 , that can inhibit reduction. The reduction of $[AuL_2^1]^+$ is an expected result because the chelation of the Au^I metal center would result in an energetically unfavorable four-membered ring; therefore, the complex is likely a preferred two coordinate Au^I complex. Further investigation of structural differences in the gold:diphosphine systems can be conducted through other selective reduction reactions.

Reaction 5 produces ligated Au^0 species, which for simplicity we term as Au^0 . The Au^0 condense to form neutral stable neutral species, $Au_{n^*}^0$, with a global rate coefficient for nucleation, k_{nc} :



Because the Au^I complexes are stable, closed shell species (assuming no aurophilic interactions) prior to their reduction, addition of an electron illustrated in reaction 5 is equivalent to a free-radical production (Au^0) process.^[4,14] Consequently, the condensation of the free radicals into clusters (reaction 6) is driven almost exclusively by the free-radical recombination reaction kinetics. Reaction 6 is treated classically as a salt reduction controlled through kinetic parameters such as temperature, stir rate, reactant addition rate, solubility, etc., but the recombination of L^n -containing free-radicals and PPh_3 -containing free-radicals do not produce similar products. The results presented below evidence that the reduction of $Au:L^n$ complexes do not follow this classic model. Further work examining the reduction and recombination mechanism is ongoing.

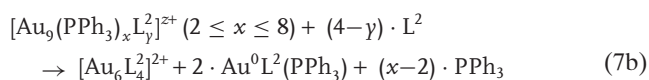
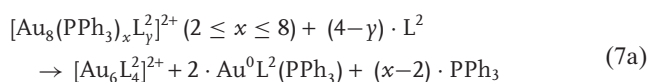
We first examine the reduction of the Class I containing gold complexes. The predominant products that form through

the reduction of the distributions of complexes containing L^2 result in a loss of ionic character in the ESI-MS, indicating the nascent cluster distribution is nearly all neutral species characterized by reaction 6. For $[L^2]/[PPh_3] = x$, $0.35 \leq x \leq 1.6$, at $t = 15$ min, the initial UV-vis spectra are characterized by only a weak, broad absorption band (Figure S4A, SI), which is consistent with previously reported $AuCIPPh_3$ reduction.^[3] At $[L^2]/[PPh_3] = 2.2$, the ESI-MS and visual appearance of the solution remains unchanged after the addition of $NaBH_4$, indicating a resistance to reduction. This represents the first demonstration of complete resistance to reduction of the Au^I :phosphine complex distribution, indicating that the rate of reaction 5 is negligible in the presence of large concentrations of highly coordinated Au^I complexes, $[AuL_2^2]^+$, (Figure 3). Therefore, because the predominant complexes in solution are always either $[Au(PPh_3)_2]^+$ or the almost irreducible $[AuL_2^2]^+$, information about the distribution of neutral clusters present can be probed.

Because the reduction observed in the $Au^I:L^2$ system is seemingly controlled by $[Au(PPh_3)_2]^+$ reduction, we employ an established colorimetric assay^[3] that probes the relative concentrations of PPh_3 -containing Au_8 and Au_9 clusters. Application of the assay at $t = 15$ min to the $[L^2]/[PPh_3] = x$, $0.35 \leq x \leq 1.0$, solution is presented in Figure 5A. For $[L^2]/[PPh_3] \approx 0.35$, which has the highest concentration of $[Au(PPh_3)_2]^+$, the presence of the 585 nm absorption band indicates a large concentration of neutral, PPh_3 -protected Au_8 and Au_9 clusters were present.^[3] These data indicate that PPh_3 -containing clusters are dominating the nascent cluster distribution, as would be predicted from the initial distribution of complexes. A fully L^2 -protected cluster distribution does not produce the 585 nm band. As $[L^2]/[PPh_3]$ increases, $[Au(PPh_3)_2]^+$ decreases (Figure 3), resulting in the decreasing intensity of the 420 nm and 585 nm bands. The overall decrease in peak intensity is in accord with lower concentrations of Au^I species being reduced, resulting from increasing concentrations

of the Au¹ trap, [AuL₂]⁺. However, it is germane to compare the assayed solutions of the Au:PPh₃ and Au:L² systems at similar time points to examine if the presence of L² provides control over nascent cluster formation. At the lowest relative L² concentration, [L²]/[PPh₃] ≈ 0.35, disparate UV–vis spectra are observed (Figure 5B), indicating that the presence of L² in the solution provides some control over the product distribution—likely through ligand exchange. The lower intensity of the 585 nm peak in the absence of L² indicates that the distribution contains predominantly PPh₃-protected clusters larger than Au₉.

The cluster distribution resulting from postreduction processing of the nascent, neutral clusters in the Au:L² system is also examined with ESI-MS and UV–vis (Figure S4, SI). At *t* = 24 h for [L²]/[PPh₃] ≈ *x*, 0.35 ≤ *x* ≤ 1.06, all UV–vis spectra contain absorption bands centered near 413 nm and 657 nm (Figure S4A), that persist for ≥ 14 days (Figure S4B, SI). The band center near 413 nm is characteristic of gold nuclearity clusters, Au_{*x*}; *x* ≥ 11.^[39] The absorption band centered near 657 nm has not been previously reported. All solutions containing the 657 nm absorption band have a corresponding *m/z* 1388 peak in the ESI-MS spectra (Figure S4C, SI), supporting a [Au₆L₄]²⁺ assignment. At [L²]/[PPh₃] = 1.6, which has the lowest [Au(PPh₃)₂]⁺ concentration prior to reduction, the 657 nm absorbance band and the *m/z* 1388 peak are absent from the spectra. These results are in accord with a predicted net reaction for [Au₆L₄]²⁺ that is similar to the reported reactions for [Au₆L₃]²⁺.^[3,40]



where the number of PPh₃ ligands present on the Au₈ and Au₉ clusters are predicted to be *x* ≥ 2 in order to promote the L² etching reaction that forms [Au₆L₄]²⁺. Because the colorimetric assay displayed a nanocluster distribution with relative large concentrations of PPh₃-containing Au₈ and Au₉ clusters (Figure 5A), it is reasonable to surmise a similar net reaction for L² can occur. The formation of [Au₆L₄]²⁺ is observed to be unique to the Class I ligands. Overall for the Au:L² system, the nascent cluster distribution results primarily from the reduction and nucleation of [Au(PPh₃)₂]⁺, as outlined in reaction 6. Subsequent solution phase processing further molds the product distribution, providing opportunity for tunable nanocluster capping and gold nuclearity.

Similar pathways of cluster formation are observed for other Class I ligand systems. The reduction of the L³ complex distribution including [Au(PPh₃)₂]⁺, [Au(PPh₃)L³]⁺ and [Au_{*x*}L³]_{*x*}⁺, by NaBH₄ results in the almost complete removal of ionic character in the ESI-MS spectra. The [AuL³]₂⁺ again shows resistance to reduction in the presence of NaBH₄. Comparing the cluster distributions present in solution at *t* < 30 min for Au:PPh₃ and the [L³]/[PPh₃] ≈ 1.0 system also exhibit differing spectra when probed with the colorimetric

assay (not shown), similar to the Au:L² system (Figure 5B). The assayed solution exhibits an intense 585 nm band relative to the 420 nm band, characteristic of larger concentrations of Au₈ and Au₉ clusters. The high concentration of neutral Au₈ and Au₉ clusters present in the L² and L³ systems compared to the broader distribution of gold nuclearities observed for Au:PPh₃ provide evidence that diphosphine ligands have stronger control over the nascent cluster distribution than PPh₃. Controlling the nascent cluster distribution, which can also be growth platforms, also allows controlled solution-phase processing for tuning final desired metal nuclearities.^[4–6,14]

The reduction behavior of the complexes also provides further information about the structure of complexes being selectively reduced. The reduction efficiency of [Au_{*x*}L³]_{*x*}⁺ is observed to be nearly 1. Complexes in Class II with similar stoichiometry always result in large concentrations of cationic clusters (vide infra), providing evidence of distinct structural differences. We recognize this could be an artifact of a distribution containing a significant population of neutral, chlorinated clusters, but this seems unlikely in the same solvent systems. Additionally, [AuL¹]₂⁺ does not exhibit the same resistance to reduction as [AuL¹]₂⁺, L^{*n*}; *n* = 2 or 3, indicating a structural difference due to ligand rigidity (Figure S5, SI). The selective reduction of these complexes with similar stoichiometry demonstrates a delicate balance between the structure of complexes and resulting nascent cluster formation, which needs further investigation.

Reduction and cluster formation in solutions containing AuClPPh₃ and ligands of Class II, L^{*n*} (*n* = 4 to 6), have the propensity to form [Au₂L^{*n*}]₂²⁺ with increasing equivalents of L^{*n*}, resulting in distinctly different clusters from those obtained with Class I ligands. At [L⁴]/[PPh₃] ≤ 0.5, [Au(PPh₃)₂]⁺ dominates the spectrum with smaller amounts of [Au₂L⁴]₂²⁺ present. Although the digold complex is a relatively small percentage of the TIC, the product formation is affected by small equivalents of L⁴, indicated by large [Au₈L⁴]₄²⁺ and [Au₁₀L⁴]₅²⁺ peak intensities at [L⁴]/[PPh₃] = 0.25 (Figure 6A). These signals are present at *t* < 30 min and persist for > 14 days. The formation of the 420 nm absorption band in the UV–vis spectra (Figure 6B) is consistent with the formation of ligated Au₈ and Au₁₀ clusters.^[1,2] Although the relative intensity of [AuL⁴]₂⁺ increases in the ESI-MS spectra from 0.5 ≤ [L⁴]/[PPh₃] ≤ 3, the principal products remain with decreasing dispersity. The absorption band centered near 420 nm from 0.5 ≤ [L⁴]/[PPh₃] ≤ 3 does not shift, indicating similar product distributions (Figure 6B). Instead, the intensity of the 420 nm absorption increases with increasing equivalents of L⁴, consistent with a narrowing product dispersity observed in the ESI-MS spectra (Figure 6A). The relative shift to less disperse product formation is in accord with decreasing amounts of [Au(PPh₃)₂]⁺, where more monodisperse product formation is directly observed with the smallest measured intensities of [Au(PPh₃)₂]⁺.

The product distribution at [L⁴]/[PPh₃] ≥ 3 displays only Au₈ and Au₁₀ clusters. The complex distribution producing the tight distribution of clusters is almost entirely [Au₂L⁴]₂²⁺ and [AuL⁴]₂⁺, following the devised relationship between nanocluster distribution and [Au(PPh₃)₂]⁺ concentration.

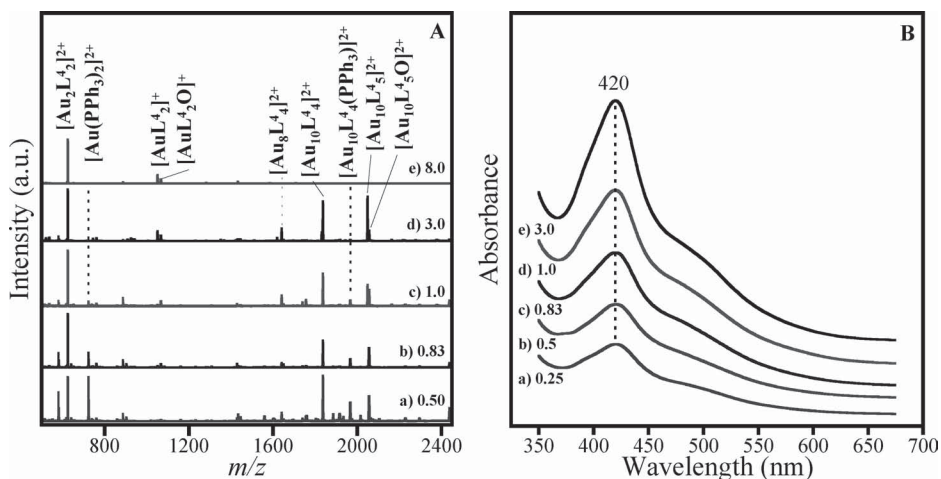
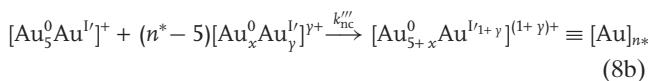
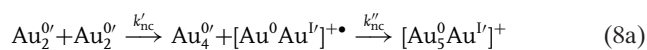


Figure 6. A) ESI-MS spectra of AuClPPH₃:L⁴ syntheses 14 days after reduction for different [L⁴]/[PPH₃]. Increasing the relative L⁴ ratio drives the cationic product formation to less polydisperse product distributions of Au₈ and Au₁₀ clusters. B) The UV-vis for the distributions represents a relatively unchanged product distribution indicated by the absorption band centered near 420 nm at all [L⁴]/[PPH₃]. UV-vis of the [L⁴]/[PPH₃] ≥ 8 did not produce stable clusters, indicated by UV-vis spectra that were similar to the unreduced synthesis solution (not shown).

Because [AuL₂]⁺ resists reduction, cluster production is formed through the reactions of fully or partially reduced [Au₂L₂]²⁺, e.g., selective reduction. The increased dispersity of the solutions with more [Au(PPH₃)₂]⁺ is consistent with the formation of a broader distribution previously reported. Interestingly, [L⁴]/[PPH₃] ≈ 8 results in the suppression of the Au:L⁴ complex distribution being reduced. The suppression of reduction for Au:L⁵ complexes is observable at [L⁵]/[PPH₃] ≥ 12 (not shown), where the [Au₂L₂]²⁺ dominates the metal-ligand complex distribution. Although the [Au₂L₂]²⁺ complex is the highest signal intensity for Lⁿ, n = 4 and 5, the presence of a significant amount of [AuLⁿ]⁺ seemingly is enough to inhibit cluster formation. [Au₂L₂]²⁺ and [Au₂L₂]²⁺ in deaerated solutions were capable of being reduced at [Lⁿ]/[PPH₃] = 8 and 12, respectively. A decrease in the fractional ion intensity of [AuLⁿ]⁺ results in the formation of mostly ligated Au₈ clusters and small amounts of Au₁₀. The initial production of cationic Au₈ and Au₁₀ clusters is observed in deaerated gold-L⁶ systems (not shown), consistent with our previous studies.^[2]

The nucleation pathways of the digold complexes are more complex than the Class I species because the reduction efficiency can either be 0, 0.5 or 1 resulting in no reduction, partial reduction ([Au⁰Au^ILⁿ]⁺) or full reduction of the complex to produce predominantly cationic clusters (Figure 6):



The order of which the cluster gains cationic character through the addition of a partially reduced digold complex ([Au⁰Au^I]⁺) can be rearranged in reactions 8, indicating that the initiation of nucleation does not have to be the addition of two Au⁰₂ species. Importantly, the nascent product has

charge. Note, Class II ligands are still available for size-selective processing, but the nascent cationic clusters appear less susceptible to size-focusing processes, such as degradation through oxidation.

The line between the specific products from Class I and II ligands can be blurred, consistent with the susceptibility of the complex distributions to ambient environments. Because of the susceptibility to oxidation of [Au₂L₂]²⁺ (vide supra), the complexes in class I and class II yield similar distributions of complexes which yield clusters of similar nuclearity. Thus, the cluster distribution becomes homogenized, containing both Class I and II character. The manipulation of the complex distribution for L⁴ also reveals this product tunability. The ability to control product formation with different protecting ligands becomes useful when tuning specific properties that are governed by the protecting ligand and not by the intrinsic properties of the metal core, e.g., catalytic specificity and reaction rates. Interestingly, the role of longer chain phosphorous containing ligands may be a route to creating other cluster nuclearities, increased product yield or tuning specific ligand-controlled properties.

Together, these data identify a predictive tool for syntheses of Au MPCs by mapping product formation through selective reduction. The complexes that form through ligand exchange are controlled by steric properties of the protecting Class I and Class II diphosphine ligands. By selectively reducing distributions of complexes, we show unique formation pathways driven by differing reduction efficiencies, which impact the reduction, nucleation, and cluster formation processes. Increasing concentrations of PPH₃-containing complexes in the distribution *prior to* reduction *always* result in a broader product distribution, indicating that diphosphine ligands tightly control reduction and subsequent nucleation products. We show that bidentate phosphine ligands can control the nascent cluster distribution as well or better than other kinetic controls in MPC syntheses.^[2] Other strong

complexing ligands such as amines, thiols or other polymers are also reported to control the distribution of oxidized metal precursors;^[41–43] therefore, we predict the reduction of these metal-ligand complexes should also have similar product control.

3. Conclusion

The current study shows predictability in gold nanocluster syntheses for a wide range of diphosphine ligands by monitoring the initial complex distribution. To develop the mechanism leading to predicative nascent product formation, we examined how i) steric contributions from the carbon-backbone length in diphosphine ligands affect the distribution of ligand-metal complexes and ii) the reduction of the specific complex distributions control nascent cluster formation. The formation of specific solution metal-ligand complexes as a function of L^n equivalents is driven by the steric constraints and flexibility of the carbon backbone as previously described. Class I and Class II ligands form predominantly $[\text{AuL}_2]^+$ and $[\text{Au}_2\text{L}_2]^{2+}$ complexes, respectively. The structural differences of the complexes directly affect the nascent cluster distribution through differing reduction efficiencies, but this relationship is currently not understood. The reduction efficiencies of the metal-ligand complexes control the initial product formation. Disparate cluster products with different protecting ligands are observed that follow the established general classification of the inherent ligand steric properties (bite angle), which can qualitatively identify structural differences of complexes being reduced with the same stoichiometry. The reduction of complexes containing Class I ligands initially form neutral, ligated Au_8 and Au_9 clusters, and Class II ligands form ligated, cationic Au_8 and Au_{10} species. The predictable, narrow distributions of nascent product formation demonstrated in the current study can be further coupled with solution phase processing methodologies to tune desired product formation. Further experimental and computational work is necessary to understand the competing forces controlling metal-ligand structure, which should provide the information necessary for rational design of other phosphine ligands.

Another important distinction is susceptibility to oxidation of the predominant complexes that are characteristic of Class I and Class II ligands. The bridged Class II complexes are more prone to oxidation, resulting in substantial changes to the distribution of complexes. The shift in the complex distribution can blur the boundaries between the ligand classes. Overall, this study provides a predictive tool for synthetic approaches of TM clusters and should be broadly applicable for other size-selective TM:ligand systems that utilize reduction of precursor complexes for cluster/nanoparticle formation.

4. Experimental Section

Synthesis and analysis operations were conducted at ambient temperature ($T = 21\text{--}24\text{ }^\circ\text{C}$). All chemicals and solvents were purchased from Sigma-Aldrich and used as delivered.^[44] Diphosphine ligands with different length alkane backbones were

examined. As stated previously, we notate diphosphine ligands as L^n , where $L^n = 1,n$ -bis(diphenylphosphino) n -alkane; for example, L^2 is 1,2-bis(diphenylphosphino)ethane. Briefly, $\text{Au}(\text{PPh}_3)\text{Cl}$ (99.9%), and L^n were dissolved in 1:1 methanol-chloroform solutions to give appropriate $[\text{L}^n]/[\text{AuClPPh}_3]$ and stirred to allow equilibration. The uncertainty (2σ) associated with the masses of the ligands is $\pm 0.0002\text{ g}$, correlating to an average 3% uncertainty in the molar ratio with less uncertainty at high molar ratios and as high as 10% at the lowest L^n concentrations. The equivalent amount L^n added to the solutions was only used to control ligand exchange. There are several general types of complexes present in solutions, which are controlled by inherent ligand properties and are illustrated in Figure 1. After equilibration, addition of $4\times$ molar excess of NaBH_4 to the solutions induced reduction of the Au^{I} :phosphine complexes. The reaction vials were crimp-sealed and mixed with a magnetic stirbar. We will refer to solutions prepared with this procedure as aerated syntheses.

Details of the colorimetric assay have been reported elsewhere, but all were conducted in deaerated systems.^[3] Briefly, the colorimetric assay can specifically probe ionic and neutral, PPh_3 -protected Au_8 and Au_9 clusters in solution by the addition of excess assay reagent, L^3 . The addition of the assay reagent promotes etching of PPh_3 -protected Au_8 and Au_9 clusters to form $[\text{Au}_6\text{L}^3_4]^{2+}$ and traps free Au^{I} in $[\text{AuL}^3_2]^+$ through ligand exchange, minimizing subsequent reactions. Because $[\text{Au}_6\text{L}^3_4]^{2+}$ has a distinct optical signature in the UV-vis centered at 585 nm and conversion is nearly ideal, the relative intensity of 585 nm band represents (almost) all PPh_3 -containing Au_8 and Au_9 clusters present.

To examine the role of ambient conditions, solvent systems were purged by bubbling Ar through the reaction vials to remove dissolved oxygen. We refer to the purged reaction systems as deaerated. Similar protocol is used for aerated and deaerated syntheses. Again, the mixture of ligand complexes was allowed to equilibrate ($\approx 15\text{ min}$), dry reducing agent (NaBH_4) was quickly added, the solution again purged with argon, and the vial was crimp sealed. During these last operations the solution was temporarily stagnant. To minimize the introduction of oxygen, we used a syringe to remove samples through the septum.

As the reactions progressed, small samples were collected and diluted in methanol for analysis either by UV-vis or ESI-MS (in $10\times$ to $10\,000\times$ dilution). Samples were analyzed within $\approx 5\text{ min}$ of their dilution. UV-vis spectra of aerated solutions were collected on a Varian Cary II dual beam spectrometer.^[45] The mass spectrometer comprised an electrospray ion source (Analytica of Branford), coupled to a custom-built (by Ardara Technologies) Extrel CMS quadrupole mass spectrometer (mass range $\approx 10\text{ }m/z$ to $\approx 3000\text{ }m/z$). Samples were introduced to the ESI source via direct infusion ($10\text{ }\mu\text{L}/\text{min}$) through a glass capillary, and the source was purged with $\geq 1.0\text{ mL}$ of methanol between samples. The source electrical potentials, temperature, curtain gas flow, and effusion rate were optimized to maximize ion intensities while minimizing fragmentation. Stable ion currents and the spectra presented here were obtained with the potential difference between the capillary exit and the skimmer set to 80 V; however, to assure data quality and consistency, additional spectra were systematically collected for voltages between 60 and 140 V. Assignment of cluster species in ESI-MS spectra were made based on predictions of polyhedral skeletal electron pair (PSEP) theory^[46–48] and covalent labeling in

O containing complexes. Some solutions were examined for negative ions; only Cl⁻ was observed.

Supporting Information

Supporting Information, which includes colored versions of the figures, is available from the Wiley Online Library or from the author.

Acknowledgements

JMP acknowledges the NRC Fellowship for funding support.

- [1] M. F. Bertino, Z. M. Sun, R. Zhang, L. S. Wang, *J. Phys. Chem. B* **2006**, *110*, 21416.
- [2] J. M. Pettibone, J. W. Hudgens, *J. Phys. Chem. Lett.* **2010**, *1*, 2536.
- [3] J. M. Pettibone, J. W. Hudgens, *ACS Nano* **2011**, *5*, 2989.
- [4] J. M. Pettibone, J. W. Hudgens, *Phys. Chem. Chem. Phys.*, DOI:10.1039/C2CP22865C.
- [5] Y. Shichibu, K. Konishi, *Small* **2010**, *6*, 1216.
- [6] Y. Kamei, Y. Shichibu, K. Konishi, *Angew. Chem. Int. Edit.* **2011**, *50*, 7442.
- [7] R. Jin, H. Qian, Z. Wu, Y. Zhu, M. Zhu, A. Mohanty, N. Garg, *J. Phys. Chem. Lett.* **2010**, 2903.
- [8] D. E. Bergeron, O. Coskuner, J. W. Hudgens, C. A. Gonzalez, *J. Phys. Chem. C* **2008**, *112*, 12808.
- [9] T. G. Schaaff, R. L. Whetten, *J. Phys. Chem. B* **1999**, *103*, 9394.
- [10] H. F. Qian, M. Z. Zhu, E. Lanni, Y. Zhu, M. E. Bier, R. C. Jin, *J. Phys. Chem. C* **2009**, *113*, 17599.
- [11] H. W. Duan, S. M. Nie, *J. Am. Chem. Soc.* **2007**, *129*, 2412.
- [12] T. Soejima, N. Kimizuka, *J. Am. Chem. Soc.* **2009**, *131*, 14407.
- [13] S. Hong, G. Shafai, M. Bertino, T. S. Rahman, *J. Phys. Chem. C* **2011**, *115*, 14478.
- [14] J. W. Hudgens, J. M. Pettibone, T. P. Senftle, R. N. Bratton, *Inorg. Chem.* **2011**, *50*, 10178.
- [15] R. Colton, K. L. Harrison, Y. A. Mah, J. C. Traeger, *Inorg. Chim. Acta* **1995**, *231*, 65.
- [16] P. Dierkes, P. van Leeuwen, *J. Chem. Soc.-Dalton Trans.* **1999**, 1519.
- [17] P. W. N. M. van Leeuwen, P. C. J. Kamer, J. N. H. Reek, P. Dierkes, *Chem. Rev.* **2000**, *100*, 2741.
- [18] Z. Freixa, P. van Leeuwen, *J. Chem. Soc., Dalton Trans.* **2003**, 1890.
- [19] B. Chaudret, B. Delavaux, R. Poilblanc, *Coord. Chem. Rev.* **1988**, *86*, 191.
- [20] S. J. Berners-Price, M. A. Mazid, P. J. Sadler, *J. Chem. Soc.-Dalton Trans.* **1984**, 969.
- [21] H. Schmidbaur, A. Schier, *Chem. Soc. Rev.* **2008**, *37*, 1931.
- [22] P. Schwerdtfeger, H. L. Hermann, H. Schmidbaur, *Inorg. Chem.* **2003**, *42*, 1334.
- [23] Although steric contributions may dominate formation, the steric hindrance will in turn change the overlapping of the bonding orbitals and change the electronic structure of the products.
- [24] C. A. Tolman, *J. Am. Chem. Soc.* **1970**, *92*, 2956.
- [25] C. A. Tolman, *Chem. Rev.* **1977**, *77*, 313.
- [26] C. P. Casey, G. T. Whiteker, *Isr. J. Chem.* **1990**, *30*, 299.
- [27] T. Nicksch, H. Gorus, W. Weigand, *Eur. J. Inorg. Chem.* **2010**, 95.
- [28] J. W. Raebiger, A. Miedaner, C. J. Curtis, S. M. Miller, O. P. Anderson, D. L. DuBois, *J. Am. Chem. Soc.* **2004**, *126*, 5502.
- [29] A. Pintado-Alba, H. de la Riva, M. Nieuwhuyzen, D. Bautista, P. R. Raithby, H. A. Sparkes, S. J. Teat, J. M. Lopez-de-Luzuriaga, M. C. Lagunas, *J. Chem. Soc., Dalton Trans.* **2004**, 3459.
- [30] F. Scherbaum, A. Grohmann, B. Huber, C. Krüger, H. Schmidbaur, *Angew. Chem. Int. Edit.* **1988**, *27*, 1544.
- [31] P. Pyykko, F. Mendizabal, *Inorg. Chem.* **1998**, *37*, 3018.
- [32] P. Pyykko, Y. F. Zhao, *Angew. Chem. Int. Edit.* **1991**, *30*, 604.
- [33] H. Schmidbaur, W. Graf, G. Muller, *Angew. Chem. Int. Edit.* **1988**, *27*, 417.
- [34] H. Schmidbaur, *Gold Bull.* **1990**, *23*, 11.
- [35] C. King, J. C. Wang, M. N. I. Khan, J. P. Fackler, *Inorg. Chem.* **1989**, *28*, 2145.
- [36] H. X. Zhang, C. M. Che, *Chem. Eur. J.* **2001**, *7*, 4887.
- [37] J. D. E. T. Wilton-Ely, A. Schier, N. W. Mitzel, H. Schmidbaur, *Inorg. Chem.* **2001**, *40*, 6266.
- [38] Importantly, the complexes forming with other transition metals with the same Lⁿ can deviate from the complex distributions presented in the current study, indicating that the P-M interactions are important as would be expected. Well designed experimental and theoretical studies are still necessary to elucidate the specific steric and electronic contributions for predicting the complex formation, which has still not been achieved, therefore, experimental studies identifying the complex distribution are currently preferred for determining other metal-ligand complex distributions.
- [39] K. P. Hall, D. M. P. Mingos, *Prog. Inorg. Chem.* **1984**, *32*, 237.
- [40] J. W. A. van der Velden, J. J. Bour, J. J. Steggerda, P. T. Beurskens, M. Roseboom, J. H. Noordik, *Inorg. Chem.* **1982**, *21*, 4321.
- [41] E. E. Foos, M. E. Twigg, A. W. Snow, M. G. Ancona, *J. Cluster. Sci.* **2008**, *19*, 573.
- [42] U. B. Steiner, P. Neuenschwander, W. R. Caseri, U. W. Suter, F. Stucki, *Langmuir* **19928**, 90.
- [43] H. Tsunoyama, H. Sakurai, T. Tsukuda, *Chem. Phys. Lett.* **2006**, *429*, 528.
- [44] Certain commercial materials and equipment are identified in this paper in order to adequately specify the experimental procedure. Such identification neither implies recommendation or endorsement by the National Institute of Standards and Technology nor does it imply that the material or equipment identified is the best available for the purpose.
- [45] A. Rapallo, G. Rossi, R. Ferrando, A. Fortunelli, B. C. Curley, L. D. Lloyd, G. M. Tarbuck, R. L. Johnston, *J. Chem. Phys.* **2005**, *122*.
- [46] R. B. King, *Inorg. Chim Acta* **1986**, *116*, 109.
- [47] D. M. P. Mingos, *Polyhedron* **1984**, *3*, 1289.
- [48] D. M. P. Mingos, T. Slee, L. Zhenyang, *Chem. Rev.* **1990**, *90*, 383.

Received: August 8, 2011
 Revised: October 9, 2011
 Published online: